

CIAO^{*}: MPC-based Safe Motion Planning in Predictable Dynamic Environments

Tobias Schoels^{*,**} Per Rutquist^{*} Luigi Palmieri^{**}
 Andrea Zanelli^{*} Kai O. Arras^{**} Moritz Diehl^{*,***}

^{*} *Department of Microsystems Engineering, University of Freiburg*
 (e-mail: {tobias.schoels, per.rutquist, andrea.zanelli,
 moritz.diehl}@imtek.uni-freiburg.de)

^{**} *Robert Bosch GmbH, Corporate Research, Stuttgart, Germany*
 (e-mail: {tobias.schoels, luigi.palmieri, kaioliver.arras}@de.bosch.com)

^{***} *Department of Mathematics, University of Freiburg*

Abstract: Robots have been operating in dynamic environments and shared workspaces for decades. Most optimization based motion planning methods, however, do not consider the movement of other agents, e.g. humans or other robots, and therefore do not guarantee collision avoidance in such scenarios. This paper builds upon the Convex Inner ApprOximation (CIAO) method and proposes a motion planning algorithm that guarantees collision avoidance in predictable dynamic environments. Furthermore it generalizes CIAO's free region concept to arbitrary norms and proposes a cost function to approximate time-optimal motion planning. The proposed method, CIAO^{*}, finds kinodynamically feasible and collision free trajectories for constrained robots using a model predictive control (MPC) framework and accounts for the predicted movement of other agents. The experimental evaluation shows that CIAO^{*} reaches close to time optimal behavior.

Keywords: time optimal control, safety, convex optimization, predictive control, trajectory and path planning, motion control, autonomous mobile robots, dynamic environments

1. INTRODUCTION

Safe and smooth robot navigation is still an open challenge particularly for autonomous systems navigating in shared spaces with humans (e.g. intra-logistic and service robotics) and in densely crowded environments (Triebel et al., 2016). In these scenarios, the reactive avoidance of dynamic obstacles is an important requirement. Combined with the objective of reaching time-optimal robot behavior, this poses a major challenge for motion planning and control and remains subject of active research.

Recent approaches tackle the obstacle avoidance problem by formulating and solving an optimization problem (Schulman et al., 2014; Bonalli et al., 2019; Schoels et al., 2019). These approaches offer good performance for finding locally optimal solutions but the global optimum is generally hard to find, as opposed to asymptotically optimal sampling-based planners, cf. Karaman and Frazzoli (2011). A shortcoming of most common trajectory optimization methods is that they are incapable of respecting dynamic obstacles and kinodynamic constraints, e.g. bounds on the acceleration, and typically lack a notion of time in their predictions (Quinlan and Khatib, 1993;

^{*} pronounced 'ciao-star', where ^{*} is a wildcard that specifies the norm used for the convex free region.

This research was supported by the German Federal Ministry for Economic Affairs and Energy (BMWi) via eco4wind (0324125B) and DyConPV (0324166B), by DFG via Research Unit FOR 2401, and the EUs Horizon 2020 research and innovation program under grant agreement No 732737 (ILIAD).

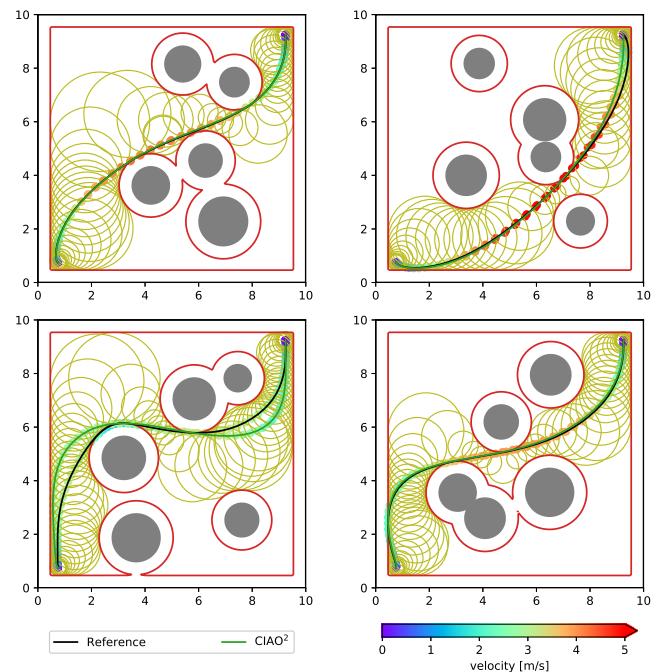


Fig. 1. Example trajectories found by CIAO² in green and a time optimal reference in black. The olive colored circles mark the convex free regions (CFRs), the red lines the safety margin to obstacles ρ .

Zucker et al., 2013; Schulman et al., 2014). These approaches are typically limited to the optimization of paths rather than trajectories and impose constraints by introducing penalties. The increase of computing power and the availability of fast numerical solvers, as for example discussed by Kouzoupis et al. (2018), has given rise to model predictive control (MPC) based approaches.

Related Work: Classical approaches to obstacle avoidance include (Borenstein and Koren, 1991; Fox et al., 1997; Ko and Simmons, 1998; Fiorini and Shiller, 1998; Minguez and Montano, 2004; Quinlan and Khatib, 1993). In contrast to our approach, they do neither produce optimal trajectories, nor account for complex robot dynamics, nor handle the obstacles with their full shape (i.e. with convex hulls) and predicted future movements.

Popular recent optimization based methods include CHOMP (Zucker et al., 2013), TrajOpt (Schulman et al., 2014), OBCA (Zhang et al., 2017), and GuSTO (Bonalli et al., 2019), which have been shown to efficiently produce smooth trajectories in static environments.

An increasing number of approaches use MPC based formulations, e.g. (Zhang et al., 2017; Bonalli et al., 2019; Herbert et al., 2017; Zhang et al., 2017), to obtain kinodynamically feasible trajectories. In this framework an optimal control problem (OCP) is solved in every iteration. The problems formulated by CIAO[★] are convex, which makes it a sequential convex programming (SCP) method like TrajOpt (Schulman et al., 2014) and GuSTO (Bonalli et al., 2019). For specific choices of ★ the formulated problems are linear, such that we obtain sequential linear programming (SLP) method, as first proposed by Griffith and Steward (1961).

Similarly to TrajOpt (Schulman et al., 2014) and GuSTO (Bonalli et al., 2019), CIAO[★] uses a signed distance function (SDF) to model the environment. While they linearize the SDF, we find a convex-inner approximation (as depicted in Fig. 1) and propose a continuous-time collision avoidance constraint, instead of a penalty term in the cost function. CIAO[★] generalizes the SDF (and thereby also the collision avoidance constraint) to arbitrary norms, similarly to OBCA (Zhang et al., 2017) and in Hyun et al. (2017). Moreover as in (Rösmann et al., 2017), it approximates time-optimal behavior.

This paper presents a generalization of CIAO, as proposed by Schoels et al. (2019). CIAO is an approach for combined obstacle avoidance and robot control that uses a convex constraint formulation that is based on the Euclidean distance to the closest obstacle. Additionally it preserves feasibility across iterations.

Contribution: In contrast to all other methods listed above, CIAO[★] guarantees collision avoidance in predictable dynamic environments. Further it differs from the original CIAO (Schoels et al., 2019) in five regards:

- CIAO[★] is norm agnostic, such that the original CIAO is a special case where ★ = 2, i.e. CIAO ≡ CIAO².
- The collision avoidance constraint is generalized to robots of shapes that can be approximated by a convex, bounding polytope.

- We motivate the use of a different cost function to approximate time optimal behavior.
- The (predicted) movement of dynamic obstacles is considered explicitly during trajectory optimization.
- We propose two generic ways of finding maximal convex free regions (CFRs).

To the best of the author’s knowledge this makes CIAO[★] the first approach that approximates time-optimal behavior in dynamic environments and guarantees collision avoidance. Like the original CIAO we present formulations for both offline trajectory optimization and online MPC based obstacle avoidance and control.

Structure: Sec. 2 formalizes the trajectory optimization problem in dynamic environments we want to solve. The proposed approach, CIAO[★], is introduced in Sec. 3 including some theoretical considerations. Sec. 4 details two algorithms that use CIAO[★] for motion planning. The experiments and results are discussed in Sec. 5. A summary and an outlook is given in Sec. 6. In App. A we introduce the *Taylor upper bound*, an approach to continuous time constraint satisfaction.

2. TIME-OPTIMAL MOTION PLANNING

We formalize time-optimal motion planning as a continuous-time optimal control problem (OCP):

$$\min_{\mathbf{x}(\cdot), \mathbf{u}(\cdot), T} T \quad (1a)$$

$$\text{s.t.} \quad 0 \leq T, \quad (1b)$$

$$\mathbf{x}(0) = \mathbf{x}_s, \quad (1c)$$

$$\mathbf{x}(T) = \mathbf{x}_g, \quad (1d)$$

$$\dot{\mathbf{x}}(t) = A\mathbf{x}(t) + B\mathbf{u}(t), \quad t \in [0, T], \quad (1e)$$

$$(\mathbf{x}(t), \mathbf{u}(t)) \in \mathcal{H}, \quad t \in [0, T], \quad (1f)$$

$$\emptyset = \text{int}(\mathcal{R}(\mathbf{x}(t))) \cap \mathcal{O}(t), \quad t \in [0, T], \quad (1g)$$

where $\mathbf{x}(\cdot) : \mathbb{R} \rightarrow \mathbb{R}^{n_x}$ denotes the robot’s state, $\mathbf{u}(\cdot) : \mathbb{R} \rightarrow \mathbb{R}^{n_u}$ is the vector of controls, T is the length of the trajectory in seconds, which is minimized. The fixed vector \mathbf{x}_s is the robot’s current state, and \mathbf{x}_g is the goal state. We use the common shorthand $\dot{\mathbf{x}}$ to denote the derivative with respect to time, i.e. $\frac{\partial \mathbf{x}}{\partial t}$. The expression $A\mathbf{x} + B\mathbf{u}$ denotes the system’s linear dynamical model, the convex polytopic set \mathcal{H} implements path constraints, e.g. physical limitations of the system. The open set $\text{int}(\mathcal{R}(\mathbf{x}(t))) \subset \mathbb{R}^n$ is the interior of the set of points occupied by the robot at time t and $\mathcal{O}(t) \subset \mathbb{R}^n$ is the set of points occupied by obstacles at that time. Finally, n is the dimension of the robot’s workspace \mathbb{R}^n . Note that for fixed T , problem (1) becomes convex if (1g) is removed.

3. CIAO[★]: CONVEX INNER APPROXIMATION

In the following we detail the reformulations and parameterizations of (1) used in this paper.

First, we introduce our implementation of the collision avoidance constraint. It is based on the concept of convex free regions (CFRs) that utilizes the signed distance function (SDF). Then we discretize (1) followed by a discussion of safety in continuous time.

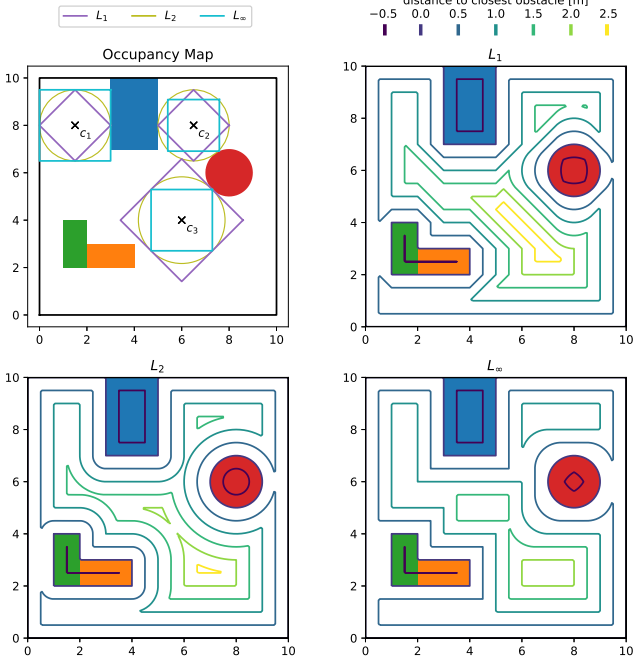


Fig. 2. Signed distance function for L_1 , L_2 , and L_∞ norm in an example environment. Top left shows the resulting convex free regions for hand picked locations.

3.1 Collision Avoidance Constraint

To formulate the collision avoidance constraint (1g) we start by introducing the signed distance function (SDF) $\text{sd}_{\mathcal{O}}^*(\cdot)$ for an arbitrary occupied set \mathcal{O} . First, we define the distance of a given point $\mathbf{p} \in \mathbb{R}^n$ to the closest occupied point $\mathbf{o} \in \mathcal{O}$ as

$$d_{\mathcal{O}}^*(\mathbf{p}) = \min_{\mathbf{o} \in \mathcal{O}} \|\mathbf{p} - \mathbf{o}\|_{\star}. \quad (2)$$

Note that $d_{\mathcal{O}}^*(\mathbf{p}) = 0$ for $\mathbf{p} \in \mathcal{O}$ and that \star is used as a wildcard, not a dual norm notation. Further, we define a measure for the penetration depth as the least distance of \mathbf{p} to any point outside the occupied set

$$\text{pen}_{\mathcal{O}}^*(\mathbf{p}) = \min_{\mathbf{o} \in \mathbb{R}^n \setminus \mathcal{O}} \|\mathbf{p} - \mathbf{o}\|_{\star}. \quad (3)$$

Note that $\text{pen}_{\mathcal{O}}^*(\mathbf{p}) = 0$ for $\mathbf{p} \notin \mathcal{O}$. We combine the two measures to obtain the SDF

$$\text{sd}_{\mathcal{O}}^*(\mathbf{p}) = d_{\mathcal{O}}^*(\mathbf{p}) - \text{pen}_{\mathcal{O}}^*(\mathbf{p}). \quad (4)$$

Note that the SDF is in general non-linear, non-convex, and non-differentiable, but continuous. An illustration of the SDF for $\star = \{1, 2, \infty\}$ is shown in Fig. 2.

The *free set* \mathcal{F}^* is the set of points that are not occupied and formally defined as

$$\mathcal{F}^* = \{\mathbf{c} \in \mathbb{R}^n : \text{sd}_{\mathcal{O}}^*(\mathbf{c}) \geq 0\}. \quad (5)$$

We can now formulate the full-body collision avoidance using the SDF by imposing $\text{int}(\mathcal{R}) \subseteq \mathcal{F}^*$.

Lemma 1. Let \mathcal{O} and \mathcal{R} be the set of points occupied by obstacles and the robot respectively, then

$$\mathcal{O} \cap \text{int}(\mathcal{R}) = \emptyset \Leftrightarrow \text{int}(\mathcal{R}) \subseteq \mathcal{F}^* \Leftrightarrow \text{sd}_{\mathcal{O}}^*(\mathbf{p}) \geq 0, \forall \mathbf{p} \in \mathcal{R}.$$

Proof: This follows directly from the definitions of the distance function (4) and the free set (5). \square

Convex Free Regions (CFRs): The collision avoidance constraint is in general non-convex, non-linear, and non-

differentiable, cf. Schulman et al. (2014). This poses a problem for derivative based optimization methods, that are used to solve the OCP in (1). To overcome this problem we use a convex inner approximation of this constraint, called convex free region (CFR).

For any point $\mathbf{c} \in \mathcal{F}^*$ the signed distance function $\text{sd}_{\mathcal{O}}^*(\mathbf{c})$ yields a *convex free region* $\mathcal{C}_{\mathbf{c}}^*$, which we define as

$$\mathcal{C}_{\mathbf{c}}^* = \{\mathbf{p} \in \mathbb{R}^n : \|\mathbf{p} - \mathbf{c}\|_{\star} \leq \text{sd}_{\mathcal{O}}^*(\mathbf{c})\}. \quad (6)$$

Note that CFR $\mathcal{C}_{\mathbf{c}}^*$ is fully described by its center point \mathbf{c} and the used norm \star . Fig. 2 contains illustrations of the CFR obtained for different, hand-picked points in an example environment. Now we show that CFRs are convex subsets of the free set.

Lemma 2. For any free point $\mathbf{c} \in \mathcal{F}^*$ the convex free region $\mathcal{C}_{\mathbf{c}}^*$ is a convex subset of \mathcal{F}^* , i.e. $\mathcal{C}_{\mathbf{c}}^* \subseteq \mathcal{F}^*$.

Proof: We prove this lemma in two steps. First, we observe that convex free regions are norm balls and therefore convex. Second, we show that $\mathbf{c} \in \mathcal{F}^* \Rightarrow \mathcal{C}_{\mathbf{c}}^* \subseteq \mathcal{F}^*$ by construction.

Take any $\mathbf{p} \in \mathcal{C}_{\mathbf{c}}^*$ and any $\mathbf{o} \in \mathcal{O}$, then the reverse triangle inequality yields $\|\mathbf{p} - \mathbf{o}\|_{\star} \geq \|\mathbf{o} - \mathbf{c}\|_{\star} - \|\mathbf{p} - \mathbf{c}\|_{\star}$. Since $\|\mathbf{c} - \mathbf{o}\|_{\star} \geq \text{sd}_{\mathcal{O}}^*(\mathbf{c})$ due to (4) and $-\|\mathbf{p} - \mathbf{c}\|_{\star} \geq -\text{sd}_{\mathcal{O}}^*(\mathbf{c})$ due to (6), we get $\|\mathbf{p} - \mathbf{o}\|_{\star} \geq \text{sd}_{\mathcal{O}}^*(\mathbf{c}) - \text{sd}_{\mathcal{O}}^*(\mathbf{c}) = 0$. \square

Remark 1. This is a generalization of Lem. 2 by Schoels et al. (2019) to arbitrary norms $\|\cdot\|_{\star}$.

Full body collision avoidance: To implement full-body collision avoidance efficiently we approximate the robot's shape by a convex polytope. Similarly to Schulman et al. (2014) we assume that there exists a finite set of points $\overline{\mathcal{R}} = \{\nu_1, \dots, \nu_{n_{\mathcal{R}}}\}$ such that $\mathcal{R} \subseteq \text{convhull}(\overline{\mathcal{R}})$. Collision checking can now be performed by enforcing that all vertices are inside the same free region, i.e. $\text{convhull}(\overline{\mathcal{R}}) \subseteq \mathcal{C}_{\mathbf{c}}^* \Leftrightarrow \nu_1, \dots, \nu_{n_{\mathcal{R}}} \in \mathcal{C}_{\mathbf{c}}^*$.

It is easy to show that this constraint is an inner approximation of the general collision avoidance constraint, i.e. $\text{int}(\overline{\mathcal{R}}) \subseteq \mathcal{C}_{\mathbf{c}}^* \Rightarrow \text{int}(\mathcal{R}) \subseteq \mathcal{C}_{\mathbf{c}}^* \Rightarrow \text{int}(\mathcal{R}) \subseteq \mathcal{F}^*$.

3.2 Enlarging Convex Free Regions

A convex free region (CFR) is formed around a center point $\mathbf{c} \in \mathcal{F}^*$ with radius $r = \text{sd}_{\mathcal{O}}^*(\mathbf{c})$. If \mathbf{c} approaches an obstacle the radius becomes smaller and in the limit ($r = \text{sd}_{\mathcal{O}}^*(\mathbf{c}) = 0$) the CFR collapses to a point. This results in a very restrictive collision avoidance constraint ($\|\mathbf{p} - \mathbf{c}\|_{\star} \leq r$). To avoid this problem, we grow CFRs using method proposed by Schoels et al. (2019), generalized to arbitrary norms.

We assume that $\mathbf{c} \in \mathcal{F}^{*1}$ and that the SDF ($\text{sd}_{\mathcal{O}}^*(\mathbf{c})$) can be computed for any $\mathbf{c} \in \mathbb{R}^n$. We then find a maximum CFR performing line search along a search direction $\mathbf{g} = \nabla_{\mathbf{c}} \text{sd}_{\mathcal{O}}^*(\mathbf{c})$, i.e., the SDF's gradient². Note that $\|\nabla_{\mathbf{c}} \text{sd}_{\mathcal{O}}^*(\mathbf{c})\|_{\star} = 1$ almost everywhere, except for points where it is undefined, e.g. ridges. In the latter case we stop the search immediately. We obtain the maximum step size η by solving the following optimization problem

$$\max_{\eta \geq 0} \eta \quad \text{s.t.} \quad \text{sd}_{\mathcal{O}}^*(\underbrace{\eta \cdot \mathbf{g} + \mathbf{c}}_{=\mathbf{c}^*}) = \eta + \text{sd}_{\mathcal{O}}^*(\mathbf{c}), \quad (7)$$

¹ If $\mathbf{c} \notin \mathcal{F}^*$ we follow the gradient to find a $\mathbf{c}' \in \mathcal{F}^*$.

² It is sufficient to implement $\nabla_{\mathbf{c}} \text{sd}_{\mathcal{O}}^*(\mathbf{c})$ using finite differences.

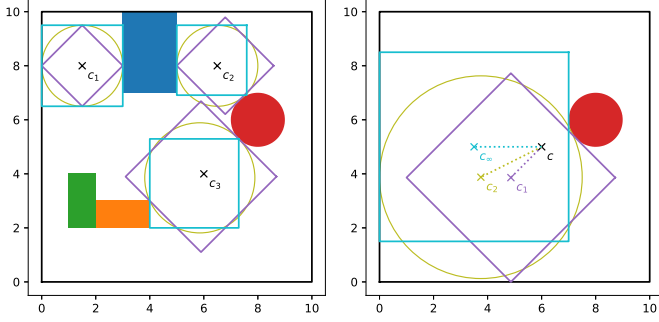


Fig. 3. Enlarged convex free regions (CFRs). Left: enlarged regions for L_1 (purple), L_2 (olive), and L_∞ (cyan) for the starting points and environment used Fig. 2. Right: the same for a simplified environment, including the corresponding center points and search direction.

where $\mathbf{c} \in \mathcal{F}^*$ is a given initial point. We obtain an enlarged CFR $\mathcal{C}_{\mathbf{c}^*}^*$ with center point $\mathbf{c}^* = \eta \cdot \mathbf{g} + \mathbf{c}$ and radius $r^* = \text{sd}_{\mathcal{O}}^*(\mathbf{c}^*)$. Note that the line search will terminate on a ridge.

Solving (7) yields a new free region $\mathcal{C}_{\mathbf{c}^*}^*$ that includes the original one $\mathcal{C}_{\mathbf{c}}^*$. When solving this problem numerically we introduce a small tolerance to allow for errors introduced by floating point arithmetic.

Lemma 3. If $\mathbf{c} \in \mathcal{F}^*$, $\mathbf{g} \in \{g \in \mathbb{R}^n : \|g\|_* = 1\}$, and $\eta \geq 0$, with $\mathbf{c}^* = \eta \cdot \mathbf{g} + \mathbf{c}$ and $\text{sd}_{\mathcal{O}}^*(\mathbf{c}^*) = \eta + \text{sd}_{\mathcal{O}}^*(\mathbf{c})$ then $\mathcal{C}_{\mathbf{c}}^* \subseteq \mathcal{C}_{\mathbf{c}^*}^*$.

Proof: We will prove this by contradiction, assuming $\exists \mathbf{p} \in \mathcal{C}_{\mathbf{c}}^*$ such that $\mathbf{p} \notin \mathcal{C}_{\mathbf{c}^*}^*$. Using (6) we rewrite our assumption to $\|(\eta \cdot \mathbf{g} + \mathbf{c}) - \mathbf{p}\|_* > \text{sd}_{\mathcal{O}}^*(\mathbf{c}^*)$. Applying the triangle inequality on the left side yields $\|\mathbf{p} - (\mathbf{c} + \eta \cdot \mathbf{g})\|_* \leq \|\mathbf{p} - \mathbf{c}\|_* + \|\eta \cdot \mathbf{g}\|_* = \|\mathbf{p} - \mathbf{c}\|_* + \eta$ and based on our assumption $\|\mathbf{p} - \mathbf{c}\|_* + \eta \leq \text{sd}_{\mathcal{O}}^*(\mathbf{c}) + \eta$ holds. Inserting this gives $\text{sd}_{\mathcal{O}}^*(\mathbf{c}) + \eta > \text{sd}_{\mathcal{O}}^*(\mathbf{c}^*)$ and thus contradicts the condition $\text{sd}_{\mathcal{O}}^*(\mathbf{c}^*) = \eta + \text{sd}_{\mathcal{O}}^*(\mathbf{c})$. \square

Remark 2. This is a generalization of Lem. 6 by Schoels et al. (2019) to arbitrary norms $\|\cdot\|_*$.

Figure 3 shows free regions produced by this line search approach in different norms.

3.3 Discrete Time OCP

Now we discretize the horizon with respect to time and obtain N uniformly spaced sampling points $t_k = k \cdot \Delta t$ for $k = 0, \dots, N$ and a chosen sampling time Δt . For more compact notation, we use the shorthand $\mathbf{x}_k = \mathbf{x}(t_k)$ to denote discrete time quantities.

Objective function: To approximate time-optimal behavior without time scaling, i.e., for a fixed Δt , we use the scheme proposed by Verschueren et al. (2017). They show that for the case of point-to-point motion, i.e., if the robot shall move from \mathbf{x}_s to \mathbf{x}_g in minimal time, the time optimal objective function can be approximated by:

$$\min_{\mathbf{x}_0, \dots, \mathbf{x}_N, \mathbf{u}_0, \dots, \mathbf{u}_{N-1}} \sum_{k=0}^{N-1} \alpha^k \|\mathbf{x}_k - \mathbf{x}_g\|$$

with initial condition $\mathbf{x}_0 = \mathbf{x}_s$ and terminal constraint $\mathbf{x}_N = \mathbf{x}_g$ for a large enough N and a large enough $\alpha > 1$, such that time optimality is recovered.

We use piece-wise constant controls, i.e. $\mathbf{u}(t) = \mathbf{u}_k$ for $t \in [t_k, t_{k+1})$ and assume that \mathbf{x}_g is a steady state at $\mathbf{u} = 0$, i.e., $0 = \mathbf{A}\mathbf{x}_g$. Note that this transformation is norm-agnostic.

Robot Model: We solve the dynamical model under for the presence of constant inputs using the matrix exponential and obtain $A_D = e^{\mathbf{A}\Delta t}$ and $B_D = \left(\int_0^{\Delta t} e^{\mathbf{A}t} dt\right) B$. The discretized dynamics are thus given by $\mathbf{x}_{k+1} = A_D \mathbf{x}_k + B_D \mathbf{u}_k$.

Occupied Set: In Sec. 3.1 we derived a convex inner approximation of the full body collision constraint that is based on the notion of an arbitrary occupied set \mathcal{O} . We exploit this formulation to derive a collision avoidance constraint formulation that generalizes to arbitrary time dependent occupied sets $\mathcal{O}(t)$. This allows us to account for dynamic obstacles. In a first step we now derive a discrete time occupied set \mathcal{O}_k for the time interval $[t_k, t_{k+1}]$.

We generally define the discrete time occupied set \mathcal{O}_k as the union of all occupied sets $\mathcal{O}(t)$ in the time interval:

$$\mathcal{O}_k = \bigcup_{t=t_k}^{t_{k+1}} \mathcal{O}(t). \quad (8)$$

Obviously the continuous time occupied set $\mathcal{O}(t)$ is contained in the discrete time occupied set \mathcal{O}_k for all $t \in [t_k, t_{k+1}]$. In the sequel we assume that the discrete time occupied set \mathcal{O}_k is known for all $k = 0, \dots, N$. This is a realistic assumption as mobile robots typically dispose of a system to estimate motion and states of surrounding agents.

Collision Avoidance Constraint: To guarantee collision avoidance in continuous time, the robot's movement needs to be accounted for. For more compact notation, we define the set of all points that are occupied by the robot in the time interval $[t_k, t_{k+1}]$ as $\Omega_k = \bigcup_{t=t_k}^{t_{k+1}} \mathcal{R}(\mathbf{x}(t))$ and introduce the shorthand $\mathcal{R}_k = \mathcal{R}(\mathbf{x}_k)$. We can now define the robot's action radius as

$$\rho_k = \max_{\mathbf{p} \in \Omega_k} d_{\mathcal{R}_k}^*(\mathbf{p}) = \max_{\mathbf{p} \in \Omega_k} \min_{\mathbf{p}' \in \mathcal{R}_k} \|\mathbf{p} - \mathbf{p}'\|_* \quad (9)$$

for $k = 0, \dots, N$.

We will now derive an upper bound of the robot's action radius using the *Taylor upper bound* introduced in App. A under the assumption that the robot is constrained to linear movement. We denote the robot's position by $\mathbf{p}(t)$ and rewrite it as $\mathbf{p}(t) = \mathbf{p}_k + \Delta \mathbf{p}(t, t_k)$. Under the assumption that the first m derivatives of \mathbf{p} with respect to time are known and that the m^{th} derivative is globally bounded by $\|\mathbf{p}^{(m)}(t)\|_* \leq \bar{p}^{(m)}, \forall t \in \mathbb{R}$, we use the Taylor upper bound and get

$$\|\Delta \mathbf{p}(t, t_k)\|_* \leq \sum_{i=1}^{m-1} \left\| \mathbf{p}_k^{(i)} \right\|_* \frac{\Delta t^i}{i!} + \bar{p}^{(m)} \frac{\Delta t^m}{m!}. \quad (10)$$

We assume that $\mathbf{p}_k^{(1)}, \dots, \mathbf{p}_k^{(m-1)}$ for $k = 0, \dots, N$ are point wise bounded, such that $\left\| \mathbf{p}_k^{(i)} \right\|_* \leq \bar{p}^{(i)}$ for $i = 1, \dots, m-1$. This yields an upper bound of the robot's action radius:

$$\|\Delta \mathbf{p}(t, t_k)\|_* \leq \rho = \sum_{i=1}^m \bar{p}^{(i)} \frac{\Delta t^i}{i!}, \quad (11)$$

for all $k = 0, \dots, N$. Note that ρ is independent of the time index k , but requires that all $\mathbf{p}_k^{(i)}$ are bounded.

Analogously to Sec. 3.1 we assume that \mathcal{R}_k can be approximated by a convex bounding polytope with vertices $\overline{\mathcal{R}}_k = \{\nu_{1,k}, \dots, \nu_{n_{\mathcal{R}},k}\}$. Due to the linear motion assumption, the vertices are given by $\nu_{i,k} = S_{\mathbf{p}} \cdot \mathbf{x}_k + l_i$, where $S_{\mathbf{p}}$ is a selector matrix, such that the robot's position is given by $\mathbf{p} = S_{\mathbf{p}} \cdot \mathbf{x}$. This allows us to formulate a convex collision avoidance constraint

$$\|\nu_{i,k} - \mathbf{c}_k\|_{\star} \leq \text{sd}_{\mathcal{O}_k}^{\star}(\mathbf{c}_k) - \rho_k \quad (12)$$

for $i = 1, \dots, n_{\mathcal{R}}$ and $k = 0, \dots, N$. Note that for a fixed \mathbf{c}_k (12) is a conic constraint in $\nu_{i,k}$ and thereby a set of conic constraints in \mathbf{x}_k . We will now show that (12) guarantees continuous time collision avoidance.

Lemma 4. Given the occupied set \mathcal{O}_k , the robot action radius $\rho \geq 0$, and a convex bounding polytope with vertices $\overline{\mathcal{R}}_k = \{\nu_{1,k}, \dots, \nu_{n_{\mathcal{R}},k}\}$ such that $\mathcal{R}_k \subseteq \text{convhull}(\overline{\mathcal{R}}_k)$, then

$$\|\nu_{i,k} - \mathbf{c}_k\|_{\star} \leq \text{sd}_{\mathcal{O}_k}^{\star}(\mathbf{c}_k) - \rho, \quad i = 1, \dots, n_{\mathcal{R}}$$

implies $\text{int}(\mathcal{R}(\mathbf{x}(t))) \cap \mathcal{O}(t) = \emptyset$ for all $t \in [t_k, t_{k+1}]$.

Proof: We prove this lemma by showing that all vertices $\nu_i(t)$ for $t \in [t_k, t_{k+1}]$ and $i = 1, \dots, n_{\mathcal{R}}$ are inside the convex free region $\mathcal{C}_{\mathbf{c}_k}^{\star}$. First, we note $\|\nu_{i,k} - \mathbf{c}_k\|_{\star} \leq \text{sd}_{\mathcal{O}_k}^{\star}(\mathbf{c}_k) - \rho \Leftrightarrow \|\nu_{i,k} - \mathbf{c}_k\|_{\star} + \rho \leq \text{sd}_{\mathcal{O}_k}^{\star}(\mathbf{c}_k)$. Further, the distance between $\nu_i(t)$ and \mathbf{c}_k is given by $\|\nu_i(t) - \mathbf{c}_k\|_{\star} = \|S_{\mathbf{p}}\mathbf{x}_k + l_i + \Delta\mathbf{p}(t, t_k) - \mathbf{c}_k\|_{\star}$. Applying the triangle inequality yields $\|\nu_i(t) - \mathbf{c}_k\|_{\star} \leq \|S_{\mathbf{p}}\mathbf{x}_k + l_i - \mathbf{c}_k\|_{\star} + \|\Delta\mathbf{p}(t, t_k)\|_{\star}$. From (9) we know $\|\Delta\mathbf{p}(t, t_k)\|_{\star} \leq \rho$, which results in $\|\nu_i(t) - \mathbf{c}_k\|_{\star} \leq \|\nu_{i,k} - \mathbf{c}_k\|_{\star} + \rho \leq \text{sd}_{\mathcal{O}_k}^{\star}(\mathbf{c}_k)$ \square

Path Constraints: To obtain continuous time constraint satisfaction for the convex polyhedral set \mathcal{H} we utilize the *Taylor upper bound* introduced in App. A. This results in a smaller, convex polyhedral set. In addition we have to impose the constraints assumed for the collision avoidance constraint above, i.e. $\|\mathbf{p}_k^{(i)}\|_{\star} \leq \bar{p}^{(i)}$ for $i = 1, \dots, m-1$ and $k = 0, \dots, N$. The resulting discrete time path constraints form again a convex polytope \mathcal{H}_D .

3.4 The CIAO* Optimization Problem

Using the reformulations detailed in the Sec. 3.3 and a multiple-shooting discretization scheme we obtain the CIAO*-NLP. It is a convex conic problem that depends on goal state \mathbf{x}_g , the initial state \mathbf{x}_s , the sampling time Δt , and the tuple of CFR center points $C = (\mathbf{c}_0, \dots, \mathbf{c}_N)$ and their respective radii $r_k = \text{sd}_{\mathcal{O}_k}^{\star}(\mathbf{c}_k) - \rho$, where ρ is the robot's action radius. The CIAO*-NLP is given by

$$\min_{\mathbf{w}} \sum_{k=0}^{N-1} \alpha^k \|\mathbf{x}_k - \mathbf{x}_g\|_{Q_x} \quad (13a)$$

$$\text{s.t. } \mathbf{x}_0 = \mathbf{x}_s, \quad (13b)$$

$$\mathbf{x}_N = \mathbf{x}_g, \quad (13c)$$

$$\mathbf{x}_{k+1} = A_D \mathbf{x}_k + B_D \mathbf{u}_k, \quad k = 0, \dots, N-1, \quad (13d)$$

$$(\mathbf{x}_k, \mathbf{u}_k) \in \mathcal{H}_D, \quad k = 0, \dots, N, \quad (13e)$$

$$\|S_{\mathbf{p}}\mathbf{x}_k + l_i - \mathbf{c}_k\|_{\star} \leq r_k, \quad i = 1, \dots, n_{\mathcal{R}}, \quad k = 0, \dots, N, \quad (13f)$$

where $\alpha > 1$ and N are both large enough such that time optimal behavior is recovered. Here $\mathbf{w} = [\mathbf{x}_0^{\top}, \mathbf{u}_0^{\top}, \dots, \mathbf{u}_{N-1}^{\top}, \mathbf{x}_N^{\top}]^{\top}$ is the vector of optimization

variables. CIAO* is norm agnostic, but for the sake of clear notation we introduce Q_x as a norm specifier. The matrices A_D, B_D result from the discretization of the model. The convex set \mathcal{H}_D guarantees continuous time constraint satisfaction of the original path constraints. The collision avoidance constraint (13f) is a reformulation of (12) that uses $\nu_{i,k} = S_{\mathbf{p}} \cdot \mathbf{x}_k + l_i$ for $i = 1, \dots, n_{\mathcal{R}}$.

Note that (13) is a linear program (LP) problem if $Q_x, \star \in \{1, \infty\}$. This is remarkable, because LPs can be solved rapidly.

3.5 The CIAO*-Iteration

In Sec. 3.1 we introduced a convex collision avoidance constraint based on convex free regions (CFRs). We will now introduce the *CIAO*-iteration* as formulated in Alg. 1.

Algorithm 1 the CIAO*-iteration

```

1: function CIAO*-ITERATION( $\mathbf{w}; \mathbf{x}_g, \mathbf{x}_s, \Delta t$ )
2:    $C \leftarrow (\mathbf{c}_k = S_{\mathbf{p}} \cdot \mathbf{x}_k \text{ for } k = 0, \dots, N)$ 
3:    $C^* \leftarrow (c^* = \text{MAXIMIZECFR}(c) \text{ for all } c \in C)$   $\triangleright$  solve (7)
4:    $\mathbf{w}^* \leftarrow \text{SOLVECIAO*-NLP}(\mathbf{w}; C^*, \mathbf{x}_g, \mathbf{x}_s, \Delta t)$   $\triangleright$  solve (13)
5: end function return  $\mathbf{w}^*$   $\triangleright$  return newly found trajectory
```

In a first step Alg. 1 obtains a tuple of center points C based on the provided initial guess \mathbf{w} (Line 2). Recall that the robots position in the workspace is given by $\mathbf{p}_k = S_{\mathbf{p}}\mathbf{x}_k$ for a selector matrix $S_{\mathbf{p}}$. The center points C are the optimized as described in Sec. 3.2 (Line 3) to formulate the CIAO*-NLP. The CIAO*-NLP is then solved using a suitable solver (Line 4).

Note that the CIAO*-iteration, as detailed above, preserves feasibility. In the case of robot motion planning (and $\gamma = 0$) that means: for a kinodynamically feasible and collision free initial guess \mathbf{w} Alg. 1 finds a kinodynamically feasible and collision free trajectory that is faster or equally quick.

4. CIAO* FOR MOTION PLANNING

In this section we discuss how the Convex Inner Approximation (CIAO*) method described in Sec. 3 can be used for motion planning. We propose two algorithms: First, an algorithm for offline trajectory optimization and a second one for online motion planning and control.

4.1 CIAO* for Trajectory Optimization

Now we consider the application of CIAO* for offline trajectory optimization. Alg. 2 finds trajectories that approximate the time optimal solution by iteratively improving a given initial guess \mathbf{w} . In a first step, we use run a single

Algorithm 2 CIAO* for offline trajectory optimization

```

Require:  $\mathbf{w}, \mathbf{x}_s, \mathbf{x}_g, \Delta t, \varepsilon$   $\triangleright$  initial guess, start and goal state
1:  $\mathbf{w}^* \leftarrow \text{CIAO*-ITERATION}(\mathbf{w}; \mathbf{x}_g, \mathbf{x}_s, \Delta t)$   $\triangleright$  see Alg. 1
2: while  $\text{COST}(\mathbf{w}^*) - \text{COST}(\mathbf{w}) > \varepsilon$  do
3:    $\mathbf{w} \leftarrow \mathbf{w}^*$   $\triangleright$  set last solution as initial guess
4:    $\mathbf{w}^* \leftarrow \text{CIAO*-ITERATION}(\mathbf{w}; \mathbf{x}_g, \mathbf{x}_s, \Delta t)$   $\triangleright$  see Alg. 1
5: end while
6: return  $\mathbf{w}^*$ 
```

CIAO*-iteration to improve the initial guess (Line 1).

While the improvement of found by CIAO^{*} with respect to a chosen cost function (e.g. CIAO^{*}'s objective function) exceeds a chosen threshold ε (Line 3), we run further CIAO^{*}-iterations (Line 3-4).

Note that Alg. 2 preserves feasibility, since the CIAO^{*}-iteration does. In other words: Once Alg. 2 converged to a feasible trajectory it will continue to find feasible (and better) trajectories only.

4.2 CIAO^{*}-MPC: Online Motion Planning

Finally we propose CIAO^{*}-MPC, an algorithms that unifies trajectory optimization and tracking, also referred to as online motion planning. To meet the time constraints the robot's control loop poses, we use a horizon of fixed length N , which is typically shorter than the one used for pure trajectory optimization (as described before). As a consequence the goal might not be reachable during the now receding horizon. Therefore we replace the terminal constraint by a Meyer term and obtain an approximation of the CIAO^{*}-NLP (13):

$$\begin{aligned} \min_{\mathbf{w}} \quad & \alpha_N \|\mathbf{x}_N - \mathbf{x}_g\|_{Q_x} + \sum_{k=0}^{N-1} \alpha^k \|\mathbf{x}_k - \mathbf{x}_g\|_{Q_x} \\ \text{s.t.} \quad & \mathbf{x}_0 = \mathbf{x}_s, \\ & S_v \mathbf{x}_N = 0, \\ & \mathbf{x}_{k+1} = A_D \mathbf{x}_k + B_D \mathbf{u}_k, \quad k = 0, \dots, N-1, \\ & (\mathbf{x}_k, \mathbf{u}_k) \in \mathcal{H}_D, \quad k = 0, \dots, N, \\ & \|S_p \mathbf{x}_k + l_i - \mathbf{c}_k\|_* \leq r_k, \quad i = 1, \dots, n_{\mathcal{R}}, \quad k = 0, \dots, N, \end{aligned} \quad (14)$$

where $\alpha_N \gg \alpha^N$ is the Meyer term's multiplier and S_v is a selector matrix that obtains the vector $\mathbf{v} = S_v \cdot \mathbf{x}$. By constraining the robot's velocity to be zero at the end of the horizon we prevent collision avoidance that could occur when receding the horizon. The above nonlinear program (NLP) replaces (13) in Line 4 of the CIAO^{*}-iteration.

Algorithm 3 CIAO^{*}-MPC

Require: \mathbf{w} , \mathbf{x}_g , Δt \triangleright initial guess, goal state, and sampling time
1: **while** $\mathbf{x}_s \neq \mathbf{x}_g$ **do** \triangleright goal reached?
2: $\mathbf{x}_s \leftarrow \text{GETCURRENTSTATE}()$
3: $\mathbf{w}^* \leftarrow \text{CIAO}^*\text{-ITERATION}(\mathbf{w}; \mathbf{x}_g, \mathbf{x}_s, \Delta t)$ \triangleright Alg. 1 with (14)
4: $\mathbf{w} \leftarrow \text{SHIFTTRAJECTORY}(\mathbf{w}^*)$ \triangleright recede horizon
5: **end while**

Alg. 3 formally introduces the CIAO^{*}-MPC approach. While the robot is not at the goal \mathbf{x}_g (Line 1), we obtain the robot's current state \mathbf{x}_s (Line 2). Next we formulate and solve (14) as described in Alg. 1 (Line 3). We conclude each iteration by shifting the trajectory \mathbf{w} (Line 4).

5. EXPERIMENTS

The performance and resulting behavior of CIAO^{*} was investigated experimentally. A first set of experiments compares trajectories found by CIAO^{*} to a time optimal reference solution. In a second set of experiments we compare the behavior of CIAO^{*} for $\star \in \{1, 2, \infty\}$. A final set of experiments evaluates CIAO^{*}-MPC's behavior. In all experiments we consider a circular robot with puck dynamics that is controlled through its jerks ($n_x = 6, n_u = 2$).

All NLPs were formulated in JuMP (Dunning et al., 2017) and solved with Gurobi on an Intel Core i7 clocked at 2.7 GHz running macOS Mojave.

	min	mean	median	max
time to goal [ratio]	1.015	1.024	1.020	1.038
path length [ratio]	0.984	0.999	1.000	1.074
control effort [ratio]	0.925	0.984	0.998	1.011
clearance [ratio]	0.999	0.999	0.999	0.999

Table 1. Evaluation of time optimal behavior approximation. We compute the normalized performance measures, obtained by taking the ratio between CIAO²'s solution and the time optimal reference (see examples in Fig. 1).

5.1 Evaluation of time-optimality

To evaluate the quality of CIAO^{*}'s approximation of time-optimal behavior, it has been tested in 50 scenarios filled with 5 circular, randomly placed obstacles with radii between 1 and 2m. The robot has to transition from a point in the lower left of the environment through the obstacles to a point in the upper right corner. The values reported in Table 1 were obtained for CIAO². We note that CIAO² finds close to time optimal trajectories. In the considered scenarios it is always less than 4% slower. The reason, why CIAO² does not fully converge to the time optimal solution can be seen in the bottom left plot of Fig. 1. The circular boundaries of the CFRs prevent motion on the safety margin (denoted by the red lines) like done by the reference in that case. We note that the average path length and control effort is even lower than the time optimal solution, meaning that CIAO^{*} finds shorter trajectories that require less control activation, but is slightly slower than the time optimal solution. At the same time it maintains the same or similar minimum distance to all obstacles, reported as clearance.

5.2 Comparison of CIAO¹, CIAO², and CIAO[∞]

For these experiments we use a similar setup as for the time optimal one. The only difference is, that the obstacles are now a mixture of circles and rectangles (both with the same probability). The experimental results reported in Tables 2 & 3 were obtained on 50 simulated scenarios.

Looking at the trajectory quality comparison in Table 2, we observe that CIAO¹, CIAO², and CIAO[∞] obtain similar results. CIAO² finds the fastest trajectories, while the shortest ones are found by CIAO¹. The reasons for these findings are visible in Fig. 4. In comparison CIAO¹ takes a more direct route at a lower average speed. It also maintains the highest clearance (measured by the Euclidean distance to the closest obstacle) due the diamond shape of the convex free region, which tied to the L_1 norm. The diamonds are quite restrictive for diagonal movement, but become comparatively large in proximity to corners allowing for smooth maneuvering around corners (see Fig. 2 & 3, c_3). The L_∞ norm on the other hand finds large regions in tunnels and corridors (see Fig. 2, c_1) and is preferred for diagonal movement, but it is restrictive in proximity to corners (see Fig. 2 & 3, c_2 & c_3) which can result in detours (see Fig. 4). The failures of CIAO¹ and CIAO[∞] result from narrow passages that these failed find a solution for due to the shape and size of their CFR.

In terms of computational efficiency CIAO[∞] reaches the best performance. This has two reasons: First, the CIAO¹-

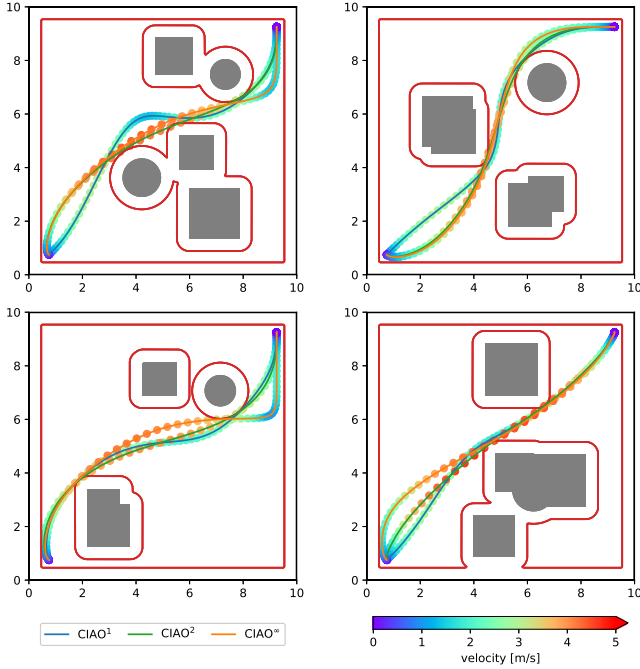


Fig. 4. CIAO* trajectories for different norms (values of \star): CIAO¹ (blue), CIAO² (green), and CIAO[∞] (orange). For CIAO² the safety margin to obstacles ρ is marked in red. Note that the safety margins for CIAO¹ & CIAO[∞] take different shapes, as depicted in Fig 2.

	CIAO ¹	CIAO ²	CIAO [∞]
success rate	96%	100%	92%
time to goal [s]	5.80 (7.40)	5.70 (6.30)	5.80 (7.20)
path length [m]	13.569 (15.338)	13.582 (15.249)	13.948 (15.429)
clearance [m]	0.294	0.262	0.262

Table 2. Trajectory quality comparison for CIAO¹, CIAO², and CIAO[∞]. We report the median (and maximum) seconds and meters in simulation (see examples in Fig. 4) of the successful scenarios.

	CIAO ¹	CIAO ²	CIAO [∞]
processing time [s]	1.709 (23.033)	1.079 (5.598)	0.656 (3.182)
iterations	26 (398)	8 (45)	10.5 (51)
time per iteration [s]	0.070 (0.112)	0.127 (0.193)	0.064 (0.098)
iterations to feasible	2 (5)	2 (4)	2 (6)

Table 3. Computational effort of CIAO¹, CIAO², and CIAO[∞] for the same experiments as in Table 2. We report the median (and maximum) computation time and iterations of the successful cases.

and CIAO[∞]-NLPs are linear programs, while the CIAO²-NLP is a second order cone program (SOCP). The latter requires more computation time to solve resulting in a higher time per iteration. Second, CIAO[∞] needs fewer iterations than CIAO¹. We note all typically find a feasible solution within the first 2 iterations and CIAO² takes at most 4 iterations, which indicates fast convergence.

	CIAO ¹	CIAO ²	CIAO [∞]
success rate	100%	100%	100%
time to goal [ratio]	1.193 (2.246)	1.037 (1.150)	1.089 (1.463)
path length [ratio]	1.014 (1.334)	0.993 (1.084)	1.014 (1.163)
control effort [ratio]	1.012 (1.428)	0.992 (1.076)	1.016 (1.267)
clearance [ratio]	1.208 (1.955)	1.004 (1.231)	1.205 (1.917)

Table 4. Trajectory quality evaluation. We report the median (and maximum) of normalized ratios between the solutions found by CIAO*-MPC and the time optimal reference.

	CIAO ¹	CIAO ²	CIAO [∞]
processing time [s]	0.058 (0.124)	0.073 (0.095)	0.043 (0.050)
solver time [s]	4.514e-04 (7.024e-04)	0.017 (0.026)	4.306e-04 (9.505e-04)

Table 5. Computational effort of CIAO*-MPC for the same experiments as in Table 4. We report the median (and maximum) computation time per MPC step.

In summary CIAO² finds the fastest trajectories and is better suited for cluttered environments. CIAO¹ and CIAO[∞] reach lower computation times per iteration, but are sensitive to the orientation and shape of obstacles. In our experiments they fail to steer the robot through some narrow passages due to the shape and size of their CFRs.

5.3 CIAO*-MPC Evaluation

To evaluate the trajectory quality lost by the approximation introduced by CIAO*-MPC, we performed experiments on the same 50 scenarios considered in Sec. 5.1. The obtained results are reported in Tables 4 & 5. We use a horizon of 50 steps resulting in a total of 406 optimization variables (plus slacks).

We observe that the trajectories found by CIAO²-MPC get closest to the time optimal reference and that they are at most 15% slower. CIAO¹ and CIAO[∞] on the other hand find less time optimal solutions, due to some detours induced by the shapes of their CFRs. This is reflected in all the path length, the time to goal and the clearance.

All, CIAO^{1,2,∞}, reach processing times less than 125 ms per MPC step (see Table 5). Only a small fraction of this time is taken up by the solver, while most it is consumed by the line search algorithm solving (7) and evaluating the distance function, which is computed online. For CIAO¹ and CIAO[∞] (14) is a LP, which yields solver times < 1 ms.

6. CONCLUSION

This paper presents CIAO*, a generalization of CIAO to dynamic environments and arbitrary norms that approximates time optimal behavior. Evaluations in simulation show that CIAO* finds close to time-optimal trajectories.

Future research will study the generalization to nonlinear systems and include considerations of uncertainty as well as a study of the convergence properties of CIAO*.

REFERENCES

Bonalli, R., Cauligi, A., Bylard, A., and Pavone, M. (2019). GuSTO: Guaranteed Sequential Trajectory Optimization via sequential convex programming. In *IEEE Int. Conf. Rob. Autom. (ICRA)*.

Borenstein, J. and Koren, Y. (1991). The vector field histogram – fast obstacle avoidance for mobile robots. *IEEE Trans. Rob. Autom.*, 7(3), 278 – 288. doi:10.1109/70.88137.

Dunning, I., Huchette, J., and Lubin, M. (2017). JuMP: A modeling language for mathematical optimization. *SIAM Review*, 59(2), 295–320. doi:10.1137/15M1020575.

Fiorini, P. and Shiller, Z. (1998). Motion planning in dynamic environments using velocity obstacles. *Int. J. Rob. Res.*, 17(7), 760–772. doi:10.1177/027836499801700706.

Fox, D., Burgard, W., and Thrun, S. (1997). The dynamic window approach to collision avoidance. *IEEE Rob. Autom. Mag.*, 4(1), 23 – 33. doi:10.1109/100.580977.

Griffith, R.E. and Steward, R.A. (1961). A nonlinear programming technique for the optimization of continuous processing systems. *Management S*, 7(4), 379–392.

Herbert, S.L., Chen, M., Han, S., Bansal, S., Fisac, J.F., and Tomlin, C.J. (2017). FaSTrack: a modular framework for fast and guaranteed safe motion planning. In *IEEE Conf. Decis. Control (CDC)*, 1517–1522. doi:10.1109/CDC.2017.8263867.

Hyun, N.s.P., Vela, P.A., and Verriest, E.I. (2017). A new framework for optimal path planning of rectangular robots using a weighted l_p norm. *IEEE Robotics and Automation Letters*, 2(3), 1460–1465.

Karaman, S. and Frazzoli, E. (2011). Sampling-based algorithms for optimal motion planning. *Int. J. Rob. Res.*, 30(7), 846–894. doi:10.1177/0278364911406761.

Ko, N.Y. and Simmons, R.G. (1998). The lane-curvature method for local obstacle avoidance. In *IEEE/RSJ Int. Conf. Intell. Rob. Syst. (IROS)*, volume 3, 1615–1621. doi:10.1109/IROS.1998.724829.

Kouzoupis, D., Frison, G., Zanelli, A., and Diehl, M. (2018). Recent advances in quadratic programming algorithms for nonlinear model predictive control. *Vietnam J. of Math.*, 46(4), 863–882.

Minguez, J. and Montano, L. (2004). Nearness diagram (nd) navigation: Collision avoidance in troublesome scenarios. *IEEE Transactions on Robotics and Automation*, 20(1), 45–59. doi:10.1109/TRA.2003.820849.

Quinlan, S. and Khatib, O. (1993). Elastic bands: Connecting path planning and control. In *IEEE Int. Conf. Rob. Autom. (ICRA)*, volume 2, 802–807. doi:10.1109/ROBOT.1993.291936.

Rösmann, C., Hoffmann, F., and Bertram, T. (2017). Integrated online trajectory planning and optimization in distinctive topologies. *Robotics and Autonomous Systems*, 88, 142–153. doi:10.1016/j.robot.2016.11.007.

Schoels, T., Palmieri, L., Arras, K.O., and Diehl, M. (2019). An NMPC approach using convex inner approximations for online motion planning with guaranteed collision freedom. *arXiv preprint arXiv:1909.08267*.

Schulman, J., Duan, Y., Ho, J., Lee, A., Awwal, I., Bradlow, H., Pan, J., Patil, S., Goldberg, K., and Abbeel, P. (2014). Motion planning with sequential convex optimization and convex collision checking. *Int. J. Rob.*

Res., 33(9), 1251–1270. doi:10.1177/0278364914528132.

Triebel, R., Arras, K., Alami, R., Beyer, L., Breuers, S., Chatila, R., Chetouani, M., Cremers, D., Evers, V., Fiore, M., et al. (2016). Spencer: A socially aware service robot for passenger guidance and help in busy airports. In *Field and service robotics*, 607–622. Springer.

Verschueren, R., Ferreau, H.J., Zananini, A., Mercangöz, M., and Diehl, M. (2017). A stabilizing nonlinear model predictive control scheme for time-optimal point-to-point motions. In *IEEE Conf. Decis. Control (CDC)*.

Zhang, X., Liniger, A., and Borrelli, F. (2017). Optimization-based collision avoidance. *arXiv preprint arXiv:1711.03449*.

Zucker, M., Ratliff, N., Dragan, A.D., Pivtoraiko, M., Klingensmith, M., Dellin, C.M., Bagnell, J.A., and Srinivasa, S.S. (2013). CHOMP: Covariant Hamiltonian Optimization for Motion Planning. *Int. J. Rob. Res.*, 32(9–10), 1164–1193. doi:10.1177/0278364913488805.

Appendix A. TAYLOR UPPER BOUND

We want to guarantee continuous time constraint satisfaction for constraints that take the form $\|p(t) - c\| \leq r$, where $p(t) \in \mathbb{R}^n$ is an m -times differentiable function w.r.t. $t \in \mathbb{R}$ and $r \in \mathbb{R}$, $c \in \mathbb{R}^n$ are constant. This problem can be approached by deriving an upper bound for the expression $\|p(t) - c\|$. In a first step we take the Taylor expansion of p around the point \bar{t} :

$$p(t) = p(\bar{t}) + \underbrace{\sum_{i=1}^{m-1} p^{(i)}(\bar{t}) \frac{(t-\bar{t})^i}{i!}}_{=\Delta p(t;\bar{t}) \text{ with } \bar{t} \in [\bar{t}, t]} + p^{(m)}(\bar{t}) \frac{(t-\bar{t})^m}{m!}, \quad (\text{A.1})$$

where $p^{(i)}(\bar{t}) = \frac{\partial^i p}{\partial t^i}(\bar{t})$ for more compact notation. Inserting (A.1) into the initial expression and applying the triangle inequality we get

$$\|p(t) - c\| = \|p(\bar{t}) - c + \Delta p(t, \bar{t})\| \quad (\text{A.2})$$

$$\leq \|p(\bar{t}) - c\| + \|\Delta p(t, \bar{t})\|. \quad (\text{A.3})$$

Under the assumption that the global upper bound of the m^{th} derivative of p is known and given by $\bar{p}^{(m)} = \max_t \|p^{(m)}(t)\|$, we obtain an upper bound for $\|\Delta p(t; \bar{t})\|$

$$\|\Delta p(t; \bar{t})\| \leq \left\| \sum_{i=1}^{m-1} p^{(i)}(\bar{t}) \frac{(t-\bar{t})^i}{i!} \right\| + \bar{p}^{(m)} \frac{\|t-\bar{t}\|^m}{m!}.$$

Assuming that $\|t - \bar{t}\|$ is bounded by $\overline{\Delta t}$ and applying the triangle inequality simplifies this expression to

$$\|\Delta p(t; \bar{t})\| \leq \sum_{i=1}^{m-1} \left\| p^{(i)}(\bar{t}) \right\| \frac{\overline{\Delta t}^i}{i!} + \bar{p}^{(m)} \frac{\overline{\Delta t}^m}{m!}. \quad (\text{A.4})$$

Finally this yields

$$\|p(t) - c\| \leq \|p(\bar{t}) - c\| + \underbrace{\sum_{i=1}^{m-1} \left\| p^{(i)}(\bar{t}) \right\| \frac{\overline{\Delta t}^i}{i!} + \bar{p}^{(m)} \frac{\overline{\Delta t}^m}{m!}}_{=\overline{\Delta p}(\bar{t}; p^{(1)}, \dots, p^{(m-1)}, \overline{\Delta t})}. \quad (\text{A.5})$$

Note that $\overline{\Delta p}(\bar{t}; p^{(1)}, \dots, p^{(m-1)}, \overline{\Delta t})$ is an upper bound on $\|\Delta p(t, \bar{t})\|$ that does not depend on t . It can thus be applied to reach continuous constraint satisfaction.